

## Electronic Mechanism that Quenches Field-Driven Heating as Illustrated with the Static Holstein Model

Manuel Weber<sup>1,2,3</sup> and James K. Freericks<sup>1</sup>

<sup>1</sup>*Department of Physics, Georgetown University, Washington, D.C. 20057, USA*

<sup>2</sup>*Max-Planck-Institut für Physik komplexer Systeme, Nöthnitzer Str. 38, 01187 Dresden, Germany*

<sup>3</sup>*Institut für Theoretische Physik and Würzburg-Dresden Cluster of Excellence ct.qmat, Technische Universität Dresden, 01062 Dresden, Germany*



(Received 8 July 2021; accepted 1 June 2023; published 29 June 2023)

Time-dependent driving of quantum systems has emerged as a powerful tool to engineer exotic phases far from thermal equilibrium, but in the presence of many-body interactions it also leads to runaway heating, so that generic systems are believed to heat up until they reach a featureless infinite-temperature state. Understanding the mechanisms by which such a heat death can be slowed down or even avoided is a major goal—one such mechanism is to drive toward an even distribution of electrons in momentum space. Here we show how such a mechanism avoids runaway heating for an interacting charge-density-wave chain with a macroscopic number of conserved quantities when driven by a strong dc electric field; minibands with nontrivial distribution functions develop as the current is prematurely driven to zero. Moreover, when approaching a zero-temperature resonance, the field strength can tune between positive, negative, or close-to-infinite effective temperatures for each miniband. Our results suggest that nontrivial metastable distribution functions should be realized in the prethermal regime of quantum systems coupled to slow bosonic modes.

DOI: 10.1103/PhysRevLett.130.266401

The possibility to induce exotic nonequilibrium states with time-dependent electromagnetic fields in solid-state systems or in optical lattices has boosted the interest in driven quantum matter [1]. A current focus has been on Floquet systems, where a time-periodic drive can realize novel topological phases [2,3] or time crystals [4–6]. Because time-dependent Hamiltonians break energy conservation, the presence of many-body interactions, like a coupling to a bath or to phonons, inevitably leads to incoherent scattering and modifies the relaxation mechanisms of the electrons [7,8]. Under which circumstances the looming heat death can be delayed [9–13] or even avoided [14–16] in a driven many-particle system is an ongoing research topic that is of immediate importance for the experimental realization of novel out-of-equilibrium phases [17,18]. For instance, the breakdown of ergodicity in the many-body-localized phase [19] has been considered as a microscopic process to avoid the heat death [14–16], but also in disorder-free realizations with a macroscopic number of conserved quantities [20]. We study the

nonequilibrium electron-phonon-coupled system, which remains too difficult to be solved exactly (for long times and large system sizes). Hence, one must make approximations that produce solutions in different limits. Here, we examine the case where the electrons interact with static phonons. This brings in limitations where heat is not directly transferred between the electrons and phonons. Nevertheless, any rapid processes occurring on electronic timescales should remain robust because once heating in the electronic system is quenched, adding energy exchange between electrons and phonons cannot significantly change the results.

In this Letter, we examine periodically driven systems that do *not* heat up indefinitely and study the logical follow-up questions: What does the steady state look like and how is it reached as a function of time? To this end, we consider a minimal interacting model where itinerant electrons on a chain are coupled to adiabatic phonons. Starting from a thermal state, we drive our system with a dc electric field, representing the simplest realization of a Floquet system (due to Bloch oscillations). This setup allows us to sample the initial states with a classical Monte Carlo method and reach the steady state on lattice sizes much larger than in state-of-the-art exact-diagonalization studies. To characterize our final states, we look at the frequency-resolved electron distribution function. In thermal equilibrium, the occupation of states is governed by the Fermi-Dirac distribution  $f_{\text{eq}}(\omega) = 1/[\exp(\beta\omega) + 1]$  and only depends

---

*Published by the American Physical Society under the terms of the Creative Commons Attribution 4.0 International license. Further distribution of this work must maintain attribution to the author(s) and the published article's title, journal citation, and DOI. Open access publication funded by the Max Planck Society.*

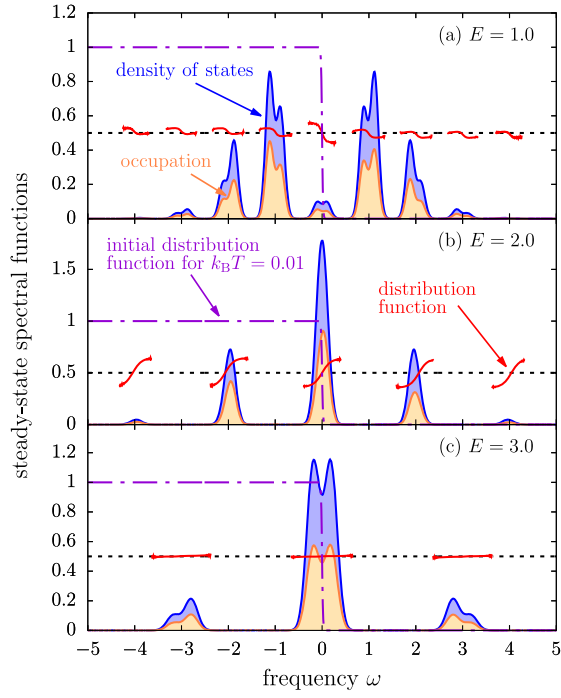


FIG. 1. Steady-state spectral functions. Density of states, occupation, and distribution function for electric field strengths of (a)  $E = 1.0$ , (b)  $E = 2.0$ , and (c)  $E = 3.0$ . Here,  $k_B T = 0.01$ ,  $L = 42$ ,  $\lambda = 0.5$ .

on the inverse temperature  $\beta = 1/k_B T$ . The fluctuation-dissipation theorem relates  $f_{\text{eq}}(\omega)$  to the ratio of lesser and retarded single-particle Green's functions (defined below). In the same way, we define a nonequilibrium distribution function  $f_{\infty}(\omega)$  for the steady state. Only if our system reaches a thermal state will  $f_{\infty}(\omega)$  correspond to  $f_{\text{eq}}(\omega)$  with a renormalized temperature. Our main results are shown in Fig. 1. The steady-state spectral functions consist of minibands centered at integer multiples of the electric field (due to the Wannier-Stark ladder formation). For each miniband, we find Fermi-Dirac-like distribution functions with negative, positive, or zero slope corresponding to positive, negative, or infinite effective temperatures, respectively. The cases with nontrivial distribution functions are highly nonequilibrium, because the distribution function should be a single one for all minibands, not a different one for each miniband; the midpoints of each miniband also follow a separate distribution function. The proximity to the heat-death scenario can be tuned by adjusting the electric field close to a zero-temperature resonance that lifts Wannier-Stark localization. Away from these points, our system never fully heats up to infinite temperature; importantly, we identify the symmetrization of the gauge-invariant momentum distribution function as the underlying mechanism to avoid the runaway heating.

To study the nontrivial properties of the steady state, we consider the 1D Holstein model  $\hat{H}(t) = \hat{H}_{\text{el}}(t) + \hat{H}_{\text{ph}}$

in an electric field. The electronic subsystem is given by

$$\hat{H}_{\text{el}}(t) = -J \sum_i (e^{-i\phi(t)} \hat{c}_i^\dagger \hat{c}_{i+1} + \text{H.c.}) + g \sum_i \hat{q}_i \left( \hat{n}_i - \frac{1}{2} \right). \quad (1)$$

The first term describes the nearest-neighbor hopping of spinless fermions with amplitude  $J$  where  $\hat{c}_i^\dagger$  ( $\hat{c}_i$ ) creates (annihilates) an electron at site  $i$ . The time-dependent flux  $\phi(t) = -Et\theta(t)$  incorporates a constant electric field  $E$  that is turned on at  $t = 0$ . We use the temporal gauge where  $\hat{H}_{\text{el}}(t)$  becomes a Floquet system with periodicity  $2\pi/E$  induced by the periodic band structure. In the second term, the local electron density  $\hat{n}_i = \hat{c}_i^\dagger \hat{c}_i$  couples to the phonon displacement  $\hat{q}_i$ . The phonon Hamiltonian reads  $\hat{H}_{\text{ph}} = \sum_i [(K/2)\hat{q}_i^2 + (1/2M)\hat{p}_i^2]$  with stiffness constant  $K$ , mass  $M$ , and momentum  $\hat{p}_i$ . We define the dimensionless coupling  $\lambda = g^2/4KJ$ , set  $e = \hbar = c = 1$ , and fix  $J = 1$  as the unit of energy. All results are for  $L = 42$  sites with periodic boundary conditions.

In this Letter, we solve the real-time dynamics of  $\hat{H}(t)$  exactly in the adiabatic limit  $M \rightarrow \infty$  of zero phonon frequency where the phonons lose their dynamics and are unable to directly exchange energy with the electrons. Then, the phonon displacements become classical variables  $\vec{q} = \{q_1, \dots, q_L\}$  and their equilibrium distribution

$$W_{\text{eq}}[\vec{q}] = \frac{1}{Z} e^{-\beta H_{\text{ph}}[\vec{q}]} Z_{\text{el}}[\vec{q}] \quad (2)$$

can be sampled using a Monte Carlo method [21,22]. Any observable  $\langle \hat{O}(t) \rangle = \int d\vec{q} W_{\text{eq}}[\vec{q}] \langle \langle \hat{O}(t) \rangle \rangle_{\vec{q}}$  of the interacting system reduces to a weighted average over noninteracting expectation values

$$\langle \langle \hat{O}(t) \rangle \rangle_{\vec{q}} = \frac{1}{Z_{\text{el}}[\vec{q}]} \text{Tr} \{ e^{-\beta(\hat{H}_{\text{el}}[\vec{q}] - \mu \hat{N})} \hat{O}_{\vec{q}}(t) \} \quad (3)$$

for a fixed  $\vec{q}$ . Here,  $Z_{\text{el}} = \text{Tr} \exp[-\beta(\hat{H}_{\text{el}} - \mu \hat{N})]$  is the partition function of the electronic subsystem with chemical potential  $\mu$  and total electron number  $\hat{N}$ . While the phonons remain static, the electronic subsystem evolves according to the Heisenberg equations of motion for  $\hat{c}_i^\dagger(t) = \hat{U}^\dagger(t, t_0) \hat{c}_i^\dagger(t_0) \hat{U}(t, t_0)$ . Because  $\hat{H}_{\text{el}}(\vec{q}, t)$  is quadratic, we only have to evolve the single-particle states using a Trotter decomposition. For a constant field  $E$ , the time-evolution operator  $\hat{U}(t, t_0)$  only needs to be calculated within its period  $\tau = 2\pi/E$ . For our simulations, we use the Trotter step  $\Delta t = 2\pi/3360 \approx 0.002$  and calculate the steady-state behavior at  $1000\tau$ . Note that, although the adiabatic limit excludes inelastic electron-phonon scattering because displacements  $\vec{q}$  are conserved, the thermal

phonon average recovers elastic electron-phonon scattering and therefore interaction effects.

We prepare our system in a thermal state with initial temperature  $k_B T$  and fix  $\lambda = 0.5$ . The phonon distribution  $W_{\text{eq}}[\vec{q}]$  is entirely determined by  $k_B T$ . At  $k_B T = 0$ , the mean-field solution  $q_i = (-1)^i \Delta/g$  is exact and leads to a band insulator with a single-particle gap  $\Delta \approx 0.3404$ . Translational symmetry is spontaneously broken by the periodic lattice distortion which gives rise to charge-density-wave order. Many-body interactions are gradually incorporated with increasing  $k_B T$ , as electrons start to scatter elastically from thermally generated phonon displacements. Already small fluctuations in the phonon fields lead to a disordered phase, but the single-particle gap is only fully filled in at  $k_B T \approx 0.1$ , where short-range charge-density-wave correlations disappear. At higher temperatures,  $W_{\text{eq}}[\vec{q}]$  eventually becomes a Gaussian with a variance  $\sigma^2 \propto k_B T$ . For further details on the equilibrium solution, see Ref. [22].

For a noninteracting system with a single band only, the application of a dc electric field leads to Bloch oscillations with periodicity  $2\pi/E$  in time-evolved observables like the electronic energy  $E_{\text{el}}(t) = \langle \hat{H}_{\text{el}}(t) \rangle / L$  or the current  $j(t) = -J \sum_i \langle i e^{-i\phi(t)} \hat{c}_i^\dagger(t) \hat{c}_{i+1}(t) + \text{H.c.} \rangle / L$ . For our clean two-band insulator at  $k_B T = 0$ , interband Zener tunneling will also populate the initially unoccupied upper band. The combination of Zener tunneling and Bragg reflections leads to very irregular oscillations [23]. For any finite initial temperature, the nonequilibrium dynamics is fundamentally different: Then, a true steady state with constant energy and zero current is reached, as we see from the transient behavior of  $E_{\text{el}}(t)$  and  $j(t)$  in Figs. 2(a) and 2(b), respectively. The damping of the average energy and current results from the destructive interference between oscillating solutions for different phonon configurations. The gauge-invariant momentum distribution function [24]  $n(k, t) = \langle \hat{c}_{k+\phi(t)}^\dagger(t) \hat{c}_{k+\phi(t)}(t) \rangle$  in Fig. 2(c) shows how the current vanishes before the system can reach an infinite-temperature state. The momentum distribution becomes a nontrivial even function of  $k$  in the long-time limit. This points toward a restoration of time-reversal symmetry in the steady state as the current is simultaneously quenched. A comparison of  $E_{\text{el}}$  between initial and final states in Fig. 2(d) reveals that heating effects are strongest at low  $k_B T$  where the steady state gets close to the infinite-temperature result  $E_{\text{el}} = 0$ . Surprisingly, a higher initial temperature reduces the final energy and thereby the effective temperature of the steady state; this is similar to the inverse Mpemba effect [25]. In addition, the steady-state occupation  $n(k)$  in Fig. 2(e) is close to a uniform distribution at low  $k_B T$  and reaches its strongest  $k$  dependence around  $k_B T = 1$ . It appears that the proximity to coherent bands at low  $k_B T$  allows for stronger heating, whereas localization effects due to phonon-induced

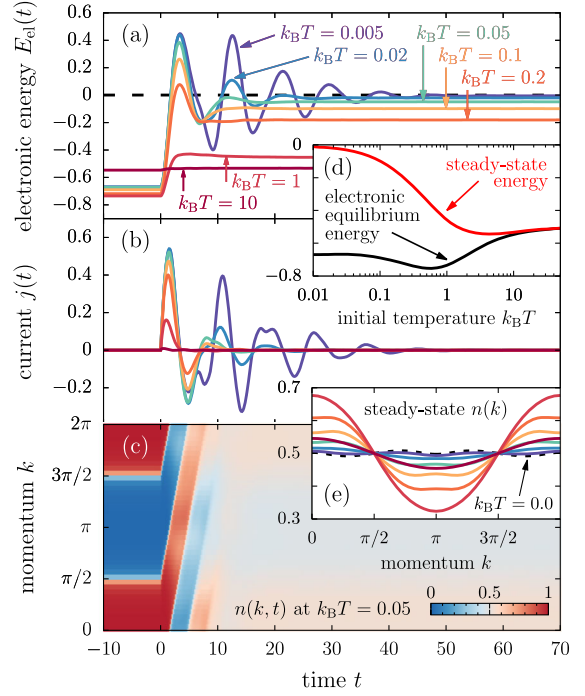


FIG. 2. Transient nonequilibrium dynamics: (a) Electronic energy and (b) current as a function of time for different initial temperatures. The dashed line in (a) represents the time average of  $E_{\text{el}}(t)$  at  $k_B T = 0$ . (c) Gauge-invariant momentum distribution function at  $k_B T = 0.05$ . (d) Comparison of the equilibrium and steady-state electronic energies as a function of temperature. (e) Steady-state momentum distribution function for different temperatures. The labels in (a) also apply to (b) and (e). Here,  $E = 1.0$ ,  $L = 42$ ,  $\lambda = 0.5$ .

disorder steadily reduce the system's ability to absorb energy with increasing  $k_B T$ . Note that  $E_{\text{el}}$  does not reach zero for  $k_B T \rightarrow \infty$ , neither in equilibrium nor for the steady state, because the variance of the phonon distribution scales as  $k_B T$  for large temperatures.

The spectral properties of the steady state can be inferred from the retarded and lesser Green's functions,

$$G_{ij}^{\text{ret}}(t, t') = -i\Theta(t - t') \langle \{ \hat{c}_i(t), \hat{c}_j^\dagger(t') \} \rangle, \quad (4)$$

$$G_{ij}^{\text{les}}(t, t') = i \langle \hat{c}_j^\dagger(t') \hat{c}_i(t) \rangle. \quad (5)$$

Using the Wigner coordinates  $t_{\text{av}} = (t + t')/2$  and  $t_{\text{rel}} = t - t'$ , we define the Fourier transform  $G_{\text{loc}}^\alpha(t_{\text{av}}, \omega) = \int dt_{\text{rel}} e^{i(\omega + i\eta)t_{\text{rel}}} \sum_i G_{ii}^\alpha(t_{\text{av}} + t_{\text{rel}}/2, t_{\text{av}} - t_{\text{rel}}/2) / L$  of the local Green's functions. Then, the density of states becomes  $A(t_{\text{av}}, \omega) = -\text{Im} G_{\text{loc}}^{\text{ret}}(t_{\text{av}}, \omega) / \pi$  and the occupation  $A^<(t_{\text{av}}, \omega) = \text{Im} G_{\text{loc}}^{\text{les}}(t_{\text{av}}, \omega) / 2\pi$ . The steady-state spectra are shown in Fig. 1 for  $k_B T = 0.01$ . Their ratio defines the nonequilibrium distribution function,

$$f_\infty(\omega) = \frac{A^<(t_{\text{av}} \rightarrow \infty, \omega)}{A(t_{\text{av}} \rightarrow \infty, \omega)}, \quad (6)$$

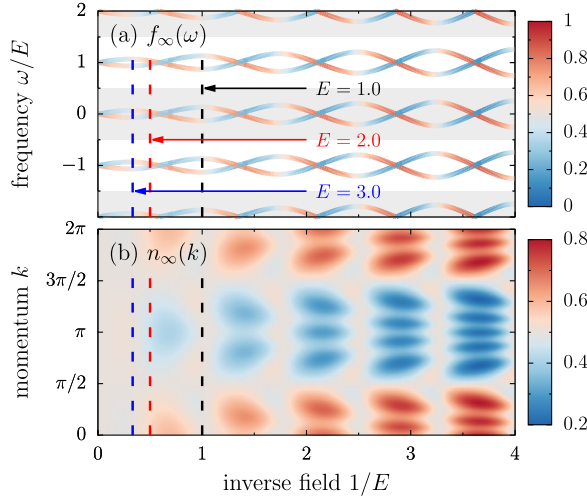


FIG. 3. Steady-state distribution functions for zero initial temperature. (a) The two quasienergies per Floquet energy window show (anti)crossings as a function of inverse field. The color coding corresponds to the spectral distribution function  $f_\infty(\omega)$ . (b) The momentum distribution function  $n_\infty(k)$  becomes flat when  $f_\infty(\epsilon_\nu) = 1/2$ . Dashed lines indicate the parameters chosen in Figs. 1 and 4. Here  $\lambda = 0.5$ .

which can be interpreted as a generalized nonequilibrium fluctuation-dissipation theorem in the long-time limit.

We can understand the main spectral features in Fig. 1 from the zero-temperature limit. Because of the doubling of the unit cell by the Peierls distortion, the energy spectrum of the steady state in Fig. 3(a) consists of two interpenetrating Wannier-Stark ladders with a level spacing of  $E$  each. The color coding of the energy levels corresponds to  $f_\infty(\omega)$ , which we calculate using Floquet theory. Because the zero-temperature Green's functions do not decay with time, we average the spectra over  $t_{\text{av}}$ ; in this way, steady-state observables are defined consistently at  $k_B T = 0$  and  $k_B T > 0$ . We obtain  $f_\infty(\epsilon_\nu + mE) = (2/L) \sum_p \langle \hat{n}_{p\nu}(t=0) \rangle$  for  $\epsilon_{1,2} \in [-E/2, E/2]$ , independent of  $m \in \mathbb{Z}$ . Here,  $\hat{n}_{p\nu}(t=0)$  is the number operator in the Floquet basis with momentum  $p \in [0, \pi)$ . Hence,  $f_\infty(\omega)$  is given by the overlap of the Floquet states with the initially occupied states. Within each Floquet energy window in Fig. 3(a), we find intervals of  $E$  where the lower (upper) band has a higher  $f_\infty$  corresponding to an effective positive (negative) temperature per miniband in Fig. 1(a) [Fig. 1(b)]. The two regimes are separated by a level crossing in the zone center as well as an avoided level crossing at the zone boundary. Zener tunneling at the avoided crossings lifts the Wannier-Stark localization and leads to an equal occupation of the two levels corresponding to an effective infinite temperature in Fig. 1(c). At these resonances, the time-averaged gauge-invariant momentum distribution function  $n_\infty(k)$  is exactly  $1/2$  for all  $k$ , as shown in Fig. 3(b) and proved in the Supplemental Material [26]. When  $1/E$  is tuned off resonance,  $n_\infty(k)$  increasingly

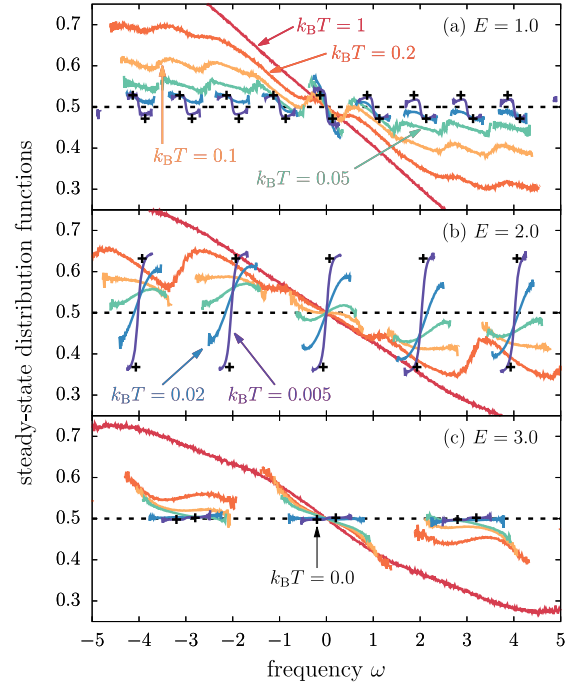


FIG. 4. Steady-state distribution functions for different initial temperatures and electric field strengths of (a)  $E = 1.0$ , (b)  $E = 2.0$ , and (c)  $E = 3.0$ . Here,  $L = 42$  and  $\lambda = 0.5$ .

gains structure with each resonance that is crossed. Resonance-induced delocalization is a well-known feature of coupled Wannier-Stark ladders [23,33] and has been observed experimentally, e.g., in semiconductor superlattices [34].

By introducing thermal fluctuations into the Floquet system via a nonzero initial  $k_B T$ , we can explain the spectral properties of Fig. 1. The phonon disorder lifts the  $L/2$ -fold degeneracy of each Floquet level such that the delta peaks in the spectra get broadened. Then, we can obtain  $f_\infty(\omega)$  on a continuous interval around the original levels as long as the spectral weight is not too small. We study the effect of the initial temperature on  $f_\infty(\omega)$  in greater detail in Fig. 4. While the distributions per miniband mainly get smeared out for positive effective temperatures in Fig. 4(a), increasing phonon fluctuations reverse the negative-temperature distributions as a function of  $k_B T$  in Fig. 4(b). The flat distributions in Fig. 4(c) remain rather flat for a broad range of  $k_B T$ . Moreover, the phonon fluctuations lift the degeneracy of  $f_\infty(\omega)$  between the different Floquet zones such that the focal points of each miniband follow an overall distribution function. As  $k_B T$  increases, the latter slowly transforms into a Fermi-Dirac-like distribution with an effective temperature that decreases. Above  $k_B T \approx 1.0$ ,  $f_\infty(\omega)$  is close to the initial thermal distribution and its effective temperature increases again, as suggested by the steady-state energy in Fig. 2(d).

We can interpret the interplay between initial temperature and electric field in terms of competing localization

mechanisms. At high temperatures, the strong Gaussian phonon disorder promotes Anderson localization. Then, the application of an electric field enhances the localization length [35], which only leads to small heating when approaching the steady state. Hence,  $f_\infty(\omega)$  becomes flatter with increasing  $E$ , as we see in Fig. 4 for  $k_B T = 1$ . Only if  $E$  is strong enough compared to the phonon disorder do signatures of Wannier-Stark localization appear, as its localization length is proportional to  $1/E$  [36]. Therefore, the steady-state features at  $k_B T \ll 1$  are governed by the Floquet solution. While each Floquet zone is populated equally at  $k_B T = 0$ , the nontrivial overall distribution for  $k_B T > 0$  seems to be a partial memory effect of  $f_{\text{eq}}(\omega)$ . We saw that heating effects are strongest at low  $k_B T$ , where the system becomes a coherent band insulator. Although observables at zero temperature never decay toward a true steady state, a time average over all  $t > 0$  is consistent with the steady-state results at  $k_B T \rightarrow 0$ , as shown in Fig. 4 for  $f_\infty(\omega)$ , in Fig. 2(a) for  $E_{\text{el}}$ , or in Fig. 2(e) for  $n_\infty(k)$  (for further data, see the Supplemental Material [26]). The higher absorption of heat at low  $k_B T$  is thus determined by an easier ability for the system to equally occupy all electronic states as time proceeds.

In conclusion, we demonstrated for a simple interacting model of itinerant electrons coupled to adiabatic phonons that the application of a dc electric field does not lead to a featureless infinite-temperature state, unless the system is tuned to a zero-temperature resonance. Instead, the heating of the electronic subsystem stops as the current is prematurely driven to zero due to the symmetrization of the momentum distribution function. We obtain strongly non-equilibrium steady states with Fermi-Dirac-like distribution functions for each Floquet miniband. These distribution functions can be tuned by the strength of the electric field, from positive to negative effective temperatures.

It remains open how quantum lattice fluctuations further affect these findings. The adiabatic phonon limit is special in the sense that electrons can only scatter elastically off the static phonon displacements. Inelastic scattering becomes important at timescales proportional to the inverse phonon frequency; for earlier times, the dynamics will be determined by the adiabatic phonon limit. For typical charge-density-wave systems, the phonons are (by several orders of magnitude) slower than the electrons. Therefore, the electron dynamics in Fig. 2 has already reached a steady state for all but the lowest temperatures before realistic phonon dynamics can set in; once the current is driven to zero via the symmetrized momentum distribution, it is unclear what could destroy this for later times. Therefore, we expect the nonequilibrium distribution functions found in this Letter to still occur for low phonon frequencies and high  $k_B T$  [37], at least in a long-lived transient regime, where elastic scattering is the dominant mechanism. Although we have identified the symmetrization of the gauge-invariant momentum distribution function in a

special setup, it will be worth studying how this mechanism affects heating in more complicated driven electron systems.

We acknowledge helpful discussions with A. Kemper and D. Luitz. This work was supported by the U.S. Department of Energy (DOE), Office of Science, Basic Energy Sciences (BES) under Award No. DE-FG02-08ER46542. Work at TU Dresden was supported by the Deutsche Forschungsgemeinschaft through the Würzburg-Dresden Cluster of Excellence on Complexity and Topology in Quantum Matter—*ct.qmat* (EXC 2147, Project No. 390858490). J. K. F. was also supported by the McDevitt bequest at Georgetown University. The authors gratefully acknowledge the Gauss Centre for Supercomputing e.V. [39] for funding this project by providing computing time on the GCS Supercomputer SuperMUC-NG at Leibniz Supercomputing Centre [40] (Project-ID pr53ju).

- 
- [1] D. N. Basov, R. D. Averitt, and D. Hsieh, Towards properties on demand in quantum materials, *Nat. Mater.* **16**, 1077 (2017).
  - [2] T. Oka and S. Kitamura, Floquet engineering of quantum materials, *Annu. Rev. Condens. Matter Phys.* **10**, 387 (2019).
  - [3] M. S. Rudner and N. H. Lindner, Band structure engineering and non-equilibrium dynamics in Floquet topological insulators, *Nat. Rev. Phys.* **2**, 229 (2020).
  - [4] V. Khemani, A. Lazarides, R. Moessner, and S. L. Sondhi, Phase Structure of Driven Quantum Systems, *Phys. Rev. Lett.* **116**, 250401 (2016).
  - [5] K. Sacha and J. Zakrzewski, Time crystals: A review, *Rep. Prog. Phys.* **81**, 016401 (2018).
  - [6] V. Khemani, R. Moessner, and S. L. Sondhi, A brief history of time crystals, [arXiv:1910.10745](https://arxiv.org/abs/1910.10745).
  - [7] L. D'Alessio and M. Rigol, Long-Time Behavior of Isolated Periodically Driven Interacting Lattice Systems, *Phys. Rev. X* **4**, 041048 (2014).
  - [8] A. Lazarides, A. Das, and R. Moessner, Equilibrium states of generic quantum systems subject to periodic driving, *Phys. Rev. E* **90**, 012110 (2014).
  - [9] D. A. Abanin, W. De Roeck, and F. Huveneers, Exponentially Slow Heating in Periodically Driven Many-Body Systems, *Phys. Rev. Lett.* **115**, 256803 (2015).
  - [10] D. V. Else, B. Bauer, and C. Nayak, Prethermal Phases of Matter Protected by Time-Translation Symmetry, *Phys. Rev. X* **7**, 011026 (2017).
  - [11] M. Bukov, M. Heyl, D. A. Huse, and A. Polkovnikov, Heating and many-body resonances in a periodically driven two-band system, *Phys. Rev. B* **93**, 155132 (2016).
  - [12] D. Abanin, W. De Roeck, W. W. Ho, and F. Huveneers, A rigorous theory of many-body prethermalization for periodically driven and closed quantum systems, *Commun. Math. Phys.* **354**, 809 (2017).
  - [13] D. J. Luitz, R. Moessner, S. L. Sondhi, and V. Khemani, Prethermalization without Temperature, *Phys. Rev. X* **10**, 021046 (2020).

- [14] A. Lazarides, A. Das, and R. Moessner, Fate of Many-Body Localization under Periodic Driving, *Phys. Rev. Lett.* **115**, 030402 (2015).
- [15] P. Ponte, Z. Papić, F. Huveneers, and D. A. Abanin, Many-Body Localization in Periodically Driven Systems, *Phys. Rev. Lett.* **114**, 140401 (2015).
- [16] D. A. Abanin, W. De Roeck, and F. Huveneers, Theory of many-body localization in periodically driven systems, *Ann. Phys. (Amsterdam)* **372**, 1 (2016).
- [17] A. Rubio-Abadal, M. Ippoliti, S. Hollerith, D. Wei, J. Rui, S. L. Sondhi, V. Khemani, C. Gross, and I. Bloch, Floquet Prethermalization in a Bose-Hubbard System, *Phys. Rev. X* **10**, 021044 (2020).
- [18] P. Peng, C. Yin, X. Huang, C. Ramanathan, and P. Cappellaro, Floquet prethermalization in dipolar spin chains, *Nat. Phys.* **17**, 444 (2021).
- [19] D. M. Basko, I. L. Aleiner, and B. L. Altshuler, Metal insulator transition in a weakly interacting many-electron system with localized single-particle states, *Ann. Phys. (Amsterdam)* **321**, 1126 (2006).
- [20] A. Smith, J. Knolle, D. L. Kovrizhin, and R. Moessner, Disorder-Free Localization, *Phys. Rev. Lett.* **118**, 266601 (2017).
- [21] K. Michielsen and H. De Raedt, Quantum molecular dynamics study of the Su-Schrieffer-Heeger model, *Z. Phys. B Condens. Mat.* **103**, 391 (1997).
- [22] M. Weber, F. F. Assaad, and M. Hohenadler, Thermodynamic and spectral properties of adiabatic Peierls chains, *Phys. Rev. B* **94**, 155150 (2016).
- [23] J. Rotvig, A.-P. Jauho, and H. Smith, Bloch Oscillations, Zener Tunneling, and Wannier-Stark Ladders in the Time Domain, *Phys. Rev. Lett.* **74**, 1831 (1995).
- [24] R. Bertoni and A. P. Jauho, Gauge-invariant formulation of the intracollisional field effect including collisional broadening, *Phys. Rev. B* **44**, 3655 (1991).
- [25] Z. Lu and O. Raz, Nonequilibrium thermodynamics of the Markovian Mpemba effect and its inverse, *Proc. Natl. Acad. Sci. U.S.A.* **114**, 5083 (2017).
- [26] See Supplemental Material at <http://link.aps.org/supplemental/10.1103/PhysRevLett.130.266401> for details on the zero-temperature solution, additional results, a discussion of interaction effects in electronic models coupled to static variables, Refs. [27–32], and data files for the results presented in this Letter.
- [27] B. M. McCoy and T. T. Wu, *The Two-Dimensional Ising Model* (Harvard University Press, Cambridge, MA and London, England, 1973).
- [28] J. K. Freericks and V. Zlatić, Exact dynamical mean-field theory of the Falicov-Kimball model, *Rev. Mod. Phys.* **75**, 1333 (2003).
- [29] O. P. Matveev, A. M. Shvaika, T. P. Devereaux, and J. K. Freericks, Stroboscopic Tests for Thermalization of Electrons in Pump-Probe Experiments, *Phys. Rev. Lett.* **122**, 247402 (2019).
- [30] M. S. Rudner and N. H. Lindner, The Floquet engineer's handbook, [arXiv:2003.08252](https://arxiv.org/abs/2003.08252).
- [31] J. H. Shirley, Solution of the Schrödinger equation with a Hamiltonian periodic in time, *Phys. Rev.* **138**, B979 (1965).
- [32] G. S. Uhrig, M. H. Kalthoff, and J. K. Freericks, Positivity of the Spectral Densities of Retarded Floquet Green Functions, *Phys. Rev. Lett.* **122**, 130604 (2019).
- [33] J. Leo and A. MacKinnon, Stark-Wannier states and Stark ladders in semiconductor superlattices, *J. Phys. Condens. Matter* **1**, 1449 (1989).
- [34] H. Schneider, H. T. Grahn, K. v. Klitzing, and K. Ploog, Resonance-Induced Delocalization of Electrons in GaAs-AlAs Superlattices, *Phys. Rev. Lett.* **65**, 2720 (1990).
- [35] V. N. Prigodin, One-dimensional disordered system in an electric field, *Zh. Eksp. Teor. Fiz.* **79**, 2338 (1980) [*Sov. Phys. JETP* **52**, 1185 (1980)].
- [36] E. Cota, J. V. José, and G. Monsiváis, Stark-ladder resonances in ordered and disordered electrified chains, *Phys. Rev. B* **35**, 8929 (1987).
- [37] In equilibrium, the adiabatic-phonon description is valid for temperatures much larger than the phonon frequency, as confirmed by exact quantum Monte Carlo simulations [38].
- [38] M. Weber, F. F. Assaad, and M. Hohenadler, Thermal and quantum lattice fluctuations in Peierls chains, *Phys. Rev. B* **98**, 235117 (2018).
- [39] [www.gauss-centre.eu](http://www.gauss-centre.eu).
- [40] [www.lrz.de](http://www.lrz.de).